ISSN: 0369-8963

Density Functional Theory (DFT) and Natural Bond Orbital (NBO) Analysis of the Interaction of Carbonyl Sulfide with Thiophene as a Gas Sensor

HARIPRIYA P [*1], AMRUTHA R [*2] and CHANDRAN P [*3]

*[*1] Research Scholar, Bharathiar University, Coimbatore, PIN-641046, Tamil Nadu, India*

*[*2]Department of Physics, KCG College of Technology, Rajiv Gandhi Salai, Karapakkam, Chennai, PIN-600097, Tamil Nadu, India*

*[*3] Madras Christian College, Tambaram East, Tambaram, Chennai, PIN-600059, Tamil Nadu, India*

[*]Corresponding author e-mail:amrutha@kcgcollege.com

ABSTRACT:

The purpose of our study is to investigate the computational calculation on the interaction of carbonyl sulfide (COS) with thiophene using density functional theory (DFT) at the B3LYP/6-31+G (d) level of theory and ωB97XD/6-31+G(d) level of theory . The adsorption energy and the counterpoise corrected energy in the most stable configuration are reported. We report that physisorbed COS act as a donor and the thiophene act as an acceptor. Computational calculations of the highest occupied molecular orbital (HOMO), the lowest unoccupied molecular orbital (LUMO), and the energy gap (E_g) are calculated and analysed. Mulliken and Natural Bond orbital (NBO) charge analysis indicate the transfer of charge from COS to monomer. By using the Molecular Electrostatic Potential (MEP), the electrophilic and nucleophilic attack properties of the complex are studied. NBO analysis is carried out to find out the distribution of charges for the monomer with the analyte and our findings show that net charge gets transferred from analyte to monomer taking into account the effect of stability on molecular structure. NBO analysis confirms the charge transfer from LP of 'O' of COS to σ of C_1-H_6 of thiophene leading to the process of adsorption. Further, the NBO analysis also explains the type of orbitals and its percentage of S-type and P-type character. Thus the adsorption of COS on thiophene is confirmed by NBO analysis. Our calculation elucidates that thiophene can be used as an excellent gas sensor for detecting COS.*

Keywords: *DFT, Thiophene, COS, Adsorption energy, HOMO-LUMO gap, MEP, NBO, Second-order perturbation*

Introduction

Gas adsorption plays an important role in the calculation of adsorption energy and the determination of charge transfer which will produce a change in the conductivity of the material. Several theoretical studies have been reported for the gas sensing behaviour of different host materials and a vast literature survey has been carried out to know about the computational calculations and analysis of gas sensing properties. DFT study at B3LYP/6-

 https://doi.org/10.37896/pd91.5/91565

ISSN: 0369-8963

31G(d) level of theory of polypyrrole both in the doped and neutral form (nPy^+/nPy) where n=3,5,7,9 with analytes NH_3, CO_2 and CO are performed to analyze the molecular and electronic structure properties of polypyrrole gas sensors with the help of electronic structure theory simulations by Salma Bibi et al. [1]. They concluded that polypyrrole has greater response with NH_3 in the presence of CO_2 and CO gases. Sensing properties of terthiophene with SO_2 and SO_3 gas molecules and their structural and electronic properties are widely studied computationally by Ali Shokuhi Rad et al. [2]. They found that the interaction energy values are proof of physical interaction between them causing complex formation. A theoretical study for Terthiophene as a model sensor for some atmospheric gases were studied by Ali shokuhi Rad revealing that polythiophene has a good potential as gas sensor toward the detection of the gases. [3]. There are handful of reported studies of conjugated organic polymers that focused on the adsorption phenomena and electronic properties produced upon interaction with various gaseous analytes. Ali Shokuhi Rad et al. presented their work on computational study for adsorptions of SO_2 and SO_3 on polyaniline (PANI) using DFT calculations. They found chemisorptions of above gaseous species. The structural and electronic properties confirm the sensing ability of 2PANI. [4] Sensing properties of conjugated organic polymers with various gas molecules and their structural and electronic properties are widely studied computationally. DFT calculations have been performed to investigate the interaction behavior of furan, pyrrole and thiophene with different gaseous analytes by Hasnain Sajid et al. [5]. To examine the components of interaction energy, symmetry-adopted perturbation theory calculations were performed by them for energy decomposition analysis to study the contribution of non-covalent components of the total interaction energy for each complex. Their result suggested that sensing ability of polypyrrole is higher than polyfuran anad polythiophene for all analytes. Ali Shokuhi Rad investigated the interaction of methanol with terthiophene (3PT) using density functional theory at BLYP-D3/6-31 +G(d,p) level of theory.[6] It is found that methanol which is highly poisonous to human beings is physisorbed by 3PT. The interactions between polythiophene and the gases NH_3, HCN, H_2S, SO_3 and H_2O at DFT were presented by Ali Shokuhi Rad et al.[7] and their analyses revealed a physisorption process for all species after interaction with 3PT. Sensitivity of polyaniline towards ammonia, carbon dioxide and carbon monoxide was studied at the unrestricted B3LYP/6-31G(d) level of theory by Habib Ullah et al. [8]. They have reported that the interaction parameters for polyaniline are more predominant for NH_3 to those of CO_2 and CO sensing. Ab-initio study of interaction of some atmospheric gases SO_2, NH_3, H_2O, CO, CH_4 and CO_2 with polypyrrole (PPy) gas sensor are computationally studied by Ali Shokuhi Rad et al. Their findings showed that a large interaction energy in 3PPy-NH_3, 3PPy-H_2O, 3PPy-SO_2, compared to less interaction energies in 3PPy-CO, 3PPy-CO_2 and 3PPy-CH_4. Their data points to PPy that will be able to use as a more appropriate sensor toward NH_3 and H_2O than other analytes.[9]. The most efficient ammonia gas sensor was obtained with a 248 nm thick polypyrrole film under electrodeposition parameters by Tilia Patois et al. [10]. Their results showed that the response was fast and reproducible at room temperataure for ammonia gas sensors based on polypyrrole films. It was shown that when detecting an electron-donating gas such as ammonia, the electric conductance of polypyrrole which is a p-ytpe conducting polymer strongly decrease. Density functional theory and TD-DFT calculations have been performed and the interaction of polypyrrole with ammonia gas sensor were extensively studied by Habib Ullah et al.[11]. It is found that the interaction of ammonia with oligopyrrole causes changes in the geometric features producing reduction in the resistance for the

 https://doi.org/10.37896/pd91.5/91565

ISSN: 0369-8963

movement of electron over the oligomer backbone. All the eletronic and geometric properties illustrate the potential of undoped oligopyrrole as sensor for ammonia. The potential of a B-doped graphene as a selective sensor for O_3, SO_2 and SO_3 molecule using DFT were investigated by Ali shokuhi Rad et al.[12]. They found weak physisorption for SO_2 and SO_3 molecule while strong chemosorption for O_3 on this surface. Performance of Intrinsic and Modified Graphene for the adsorption of Hydrogen sulfide and Methane using DFT method were analysed by Xin Gao et al. [13]. Their results revealed that hydrogen sulfide and methane show weak physical adsorption on intrinsic graphene and the energy is in the range of the physisorption process. According to their data, stronger adsorption energy results in a shorter adsorption distance with large charge transfer value. Zijia Zhao et al. explained both chemisorption and physisorption processes upon gas sensing properties of the SiC monolayer and bilayer using a Density functional theory study.[14]. The potential application of graphene as a toxic gas sensor by the adsorption of small gas molecules (CO,NO and NO_2) on (B,Al and Ga) doped graphene by ab-initio density functional theory calculations have been reported by Seba Sara Varghese et al.[15]. Electronic structure calculation of adsorbate Gas molecules on an Armchair graphene nanoribbon by Khadije Imani et al. showed the decrease of band gap after adsorbing ammonia molecule and the Fermi level shifts towards the conduction band exhibiting n-type semiconductor behavior.[16]. Recently considerable attention has been focused on gas sensing properties [17-24] by using computer simulations of different materials due to their attractive physical and chemical properties.

The band gap calculations of conjugated polymers have been extensively studied in various papers. Shujiang Yang et al. compared various molecular and solid state quantum chemical methods for their performance in predicting the band gaps of conjugated polymers.[25]. According to them, the band gap values depend strongly on the applied quantum chemical level of theory and the best values are obtained with hybrid functionals. Sanjio S.Zade and Michael Bendikov showed that the application of DFT at B3LYP/6-31G(d) level to the extrapolation of oligomer HOMO-LUMO gaps using a second – order polynomial equation is a very good method for predicting reliably the band gap of conjugated polymers.[26].

Gas sensing technology has seen good development worldwide in recent years and many kinds of sensors have been developed. The investigation of gas sensing property of monomer of polythiophene has been a growing field since it has excellences due to its properties such as high stability, easy to obtain, good mechanical properties, narrow band gap, high electrical conductivity with a lower production cost. The most promising material for gas sensing technology is thiophene which is very efficient and which is widely used in energy conversion and storage devices. The goal of our study is to elucidate the gas sensing property of thiophene with carbonyl sulfide (COS) gas using Density functional theory (DFT) methods. Density functional theory (DFT) is an effective tool for the evaluation of the structural properties of the molecule and for studying the intramolecular/intermolecular interactions. Thiophene is chosen for our study because of its simple structure and varied applications. Guangtao Li et al. formulated and synthesized Porphyrin-acetylene-thiophene polymer wires and had shown that micellar thiophene fibers gave covalent wires after oxidation.[27]. The geometries and optoelectronic properties of small conjugated compounds based on quarterthiophene and benzo[1,2,5] thiadiazole have been investigated based on the DFT B3LYP/6-31G(d) method by A.El Alamy et al.[28]. Opto electronic properties such as HOMO, LUMO, gap energy , maximum open circuit voltage (V_{oc}) suggest their materials as good candidates as active layer

 https://doi.org/10.37896/pd91.5/91565

ISSN: 0369-8963

for organic solar cells. Their findings suggested that the LUMO energies of the compounds are higher providing sufficient thermodynamic driving for electron injection from the excited compounds suggesting their materials for photovoltaic devices.[28]. Further, they found that all wavelengths calculated absorption values were inside the visible absorption solar spectrum and this factor is important for a good photovoltaic application of the molecules. Jacob H.Wat and Graham Griffin created a computer program, the computer software was written using GNU Octave 4.2 that used the optimized monomer of polythiophene and dimer to generate oligomers ranging from 1 to 166 monomer units in length. Their computational studies showed that many oligomers can be used to extrapolate the behavior of polymers and the organic semiconductors in polymeric form are used in solar cells and as energy transferring materials. [29]. DFT study of electronic and optical properties of oligothiophenes based on terthiophene end-capped by several donor groups are studied by Aziz El Alamy et al. [30].Their studies revealed that the effects of the donor group substituent on the geometries and the opto electronic properties of these materials are discussed and their work suggest some of these materials as a good candidate for organic solar cells.

Moreover, COS is the most abundant toxic sulfur compound naturally present in the atmosphere that produces acute toxicological hazards to humans and animals. [31,32]. A higher concentration of the gas can cause death resulting from respiratory paralysis. The action of COS on the nervous system is quite remarkable because COS is likely to be neurotoxic in animals and humans producing potentially irreversible peripheral neuropathy. [33]. Hence, the toxic behavior of COS, in turn, poses a large number of health hazards and environmental concerns. Hence, a gas sensor to detect COS gas is highly desirable. Further, the property of thiophene to withdraw or donate an electron to the analyte reduces the HOMO-LUMO gap that enhances high charge carrier mobility which is being very helpful in the design of organic light-emitting diodes.

Therefore in this paper, the sensitivity of thiophene with COS is reported with the help of electronic structure theory simulations. Interaction energy and counterpoise corrected energy, HOMO-LUMO analysis, band gap, molecular electrostatic potential, NBO analysis are presented in this paper. The intermolecular charge transfer between the donor and the acceptor performed in this study enable us to know about the adsorption phenomenon between COS and thiophene. The main focus of our paper is to investigate the second-order perturbation theory of Fock matrix of the NBOs that are interacting and also to analyse the population of electrons in the core, valence, and Rydberg subshells by Density functional theory. The natural bond orbital (NBO) analysis is an effective tool for the elucidation of donor-acceptor interactions in terms of Lewis structures.

In our previous work, a systematic study on the structural properties, interaction energy, and counterpoise corrected energy, dipole moment, frontier molecular orbitals, band gap, Mulliken charge transfer and natural bonding orbital (NBO) charge transfer, global reactive indices, and TD-DFT UV-vis spectral analysis have been carried out for thiophene with COS. To establish our previous work, the molecular electrostatic potential analysis, natural atomic orbital and natural bond orbital analysis of thiophene with COS have been performed in the present work. This successful computational study has validated the energetic analysis of NBO interactions by second-order perturbation theory with the DFT approach. The main scope of our work is to analyse Lewis and non-Lewis occupancies into core, valence, and Rydberg orbitals, natural

 https://doi.org/10.37896/pd91.5/91565

ISSN: 0369-8963

atomic orbitals occupancies with the percentage of hybrid atomic orbitals of most interacting NBOs that are precisely determined computationally at the B3LYP/6-31+G (d) level of theory.

Keeping all these in mind, we made a deep investigation and studied the NBO analysis of monomer with the analyte and it has been demonstrated that the calculation result of this paper is consistent with our previous work. Our successful results have shed light on the reliability of the application of thiophene in various fields of optoelectronics and become fruitful for the advancement in the field of organic electronics.

Computational method

All calculations were performed using Gaussian 09 [34] and the results were visualised and analysed using Gauss View 5.0 [35]. The density functional theory (DFT) method combined with the B3LYP/6-31+G (d) basis set is used to optimize the geometry of thiophene with COS. DFT B3LYP [36-39] (Becke3-parameter (Exchange), Lee, Yang, and Parr with a well-accepted basis set will give accurate results because of its exchange-correlation property. The most stable geometries of the complex are determined and the adsorption energies are calculated. NBO calculations are simulated at the above-mentioned level of theory.

Moreover to compare the results, we used the ωB97XD/6-31+G(d) level of theory with Grimme's D2 dispersion model [40] for optimization of structures. In general, DFT functional B3LYP/6-31+G(d) do not take dispersion arising from the fluctuation of the charge distribution around a molecular system due to the movement of the electrons, we used ωB97XD/6-31+G(d) functional. The ωB97XD functional should be sufficient because of its long-range corrected exchange-correlation behavior with the inclusion of Grimme dispersion correction.[41]. The interaction energy between monomer and analyte is calculated by the equation (2.1)

$$E_{int}=E_{complex}-(E_{monomer+}E_{analyte}) \quad \text{(2.1)}$$

The interaction energy is corrected by the counterpoise method given by (2.2)

$$E_{int,\,CP}=E_{int}-E_{BSSE} \quad \text{(2.2)}$$

where $E_{complex}$ is the relaxed energy of the optimized thiophene with COS physisorbed on it, $E_{monomer}$ is the relaxed energy of the isolated thiophene molecule, $E_{analyte}$ is the relaxed energy of the COS gas, E_{BSSE}, and $E_{int,\,CP}$ represents the basis set superposition energy error and counterpoise corrected interaction energy of the complex respectively.

Results and discussion

Interaction energy and counterpoise corrected energy

Geometries of the isolated thiophene, Carbonyl sulfide(COS), and the complex are optimized at DFT B3LYP/6-31+G(d) and are given in Figure 1(a),1(b) & 1(c) respectively. The value of interaction energy for thiophene with COS physisorbed on it is equal to -2.00832KJ/mol. This is more or less similar to that of low value obtained for H_2S adsorbed on terthiophene [7] and CH_4 adsorbed on thiophene by Hasnain Sajid et al. [5]. This low value of interaction energy is due to physisorption which is the proof of the presence of Van der Waals interaction. [7].

 https://doi.org/10.37896/pd91.5/91565

ISSN: 0369-8963

According to Xin Gao et al. stronger adsorption energy results in a shorter adsorption distance with large charge transfer value.[13] which means weaker adsorption energy results in a longer adsorption distance with a low charge transfer value. The interaction energy was corrected by counterpoise corrected energy which is given by (2.2). The counterpoise corrected energy value for the complex thiophene with COS is equal to -1.129KJ/mol which confirms that a weak intermolecular interaction has occurred. The interaction energy by DFT ωB97XD/6-31+G(d) level of theory gives -11.01979 KJ/mol. Our result shows that the interaction energy by DFT ωB97XD/6-31+G(d) level of theory is somewhat higher than DFT B3LYP/6-31+G(d) level of theory. This is because for functionals for smaller systems of 4-8 atoms, the inclusion of dispersion corrections increased the RMS error of interaction energy.[41] . By DFT ωB97XD/6-31+G(d) level of theory the counterpoise corrected interaction energy is equal to -9.498 KJ/mol. The more negative value of the interaction energy by ωB97XD/6-31+G(d) level of theory arises from the fluctuation of the charge distribution around a molecular system due to the movement of the electrons. Counterpoise correction method is used to correct the energy value because of the use of finite basis sets, BSSE (basis set superposition error) occur when atoms of interacting molecules come closer together and the basis functions of the atoms overlap each other. For weakly bound complexes, we find that the basis set superposition error energy value of 0.8816 KJ/mol of energy is observed of the order of 0.4% of interaction energy by DFT B3LYP/6-31+G(d) level of theory and a BSSE value of 1.3965 KJ/mol of energy of the order of 0.126% of E_{int} is observed for ωB97XD/6-31+G(d) level of theory.

(a)

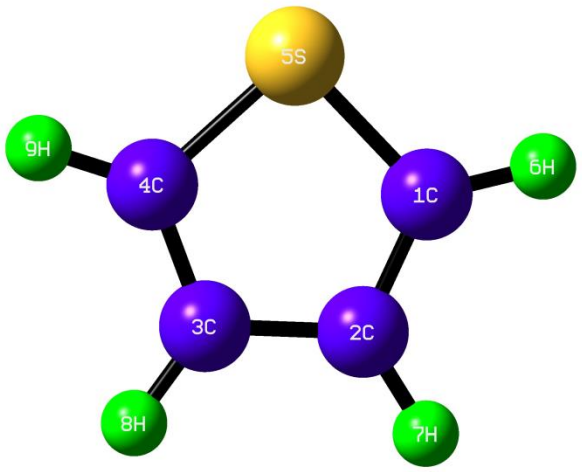

Figure 1 (a). Optimized structure of thiophene at B3LYP/6-31+G (d) level of theory

https://doi.org/10.37896/pd91.5/91565

ISSN: 0369-8963

(b)

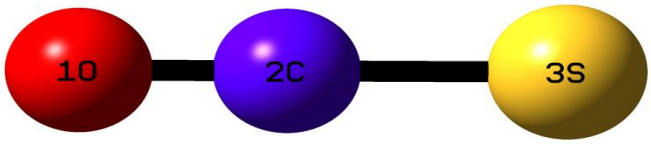

Figure 1 (b). Optimized structure of Carbonyl sulfide at B3LYP/6-31+G (d) level of theory

(c)

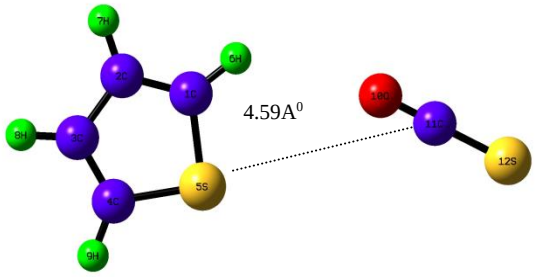

Figure 1(c). Optimized structure of thiophene with Carbonyl sulfide at B3LYP/6-31+G (d) level of theory

https://doi.org/10.37896/pd91.5/91565

ISSN: 0369-8963

TABLE 1. Interaction energy, Counterpoise corrected energy, HOMO, LUMO, band gap, charge transfer from Mulliken, and NBO analysis

S.no	Parameter	Value
1	E_{int} (KJ/mol) at B3LYP/6-31+G(d)	-2.00832
2	$E_{int, CP}$ (KJ/mol) at B3LYP/6-31+G(d)	-1.129
3	BSSE energy (KJ/mol) at B3LYP/6-31+G(d)	0.8816
4	E_{int} (KJ/mol) at ωB97XD/6-31+G(d)	-11.01979
5	$E_{int,CP}$ (KJ/mol) at ωB97XD/6-31+G(d)	-9.498
6	BSSE energy (KJ/mol) at ωB97XD/6-31+G(d)	1.3965
7	HOMO for thiophene (eV) (Molecular orbital 22)	-6.610
8	LUMO for thiophene (eV) (Molecular orbital 23)	-0.6397
9	Band gap E_g for thiophene (eV)	5.97
10	HOMO for thiophene with COS (eV) (Molecular orbital 37)	-6.5097
11	LUMO for thiophene with COS (eV) (Molecular orbital 38)	-1.297
12	Band gap E_g for thiophene with COS (eV)	5.21
13	HOMO -1 for thiophene (eV) (Molecular orbital 21)	-7.0096
14	LUMO + 1 for thiophene (eV) (Molecular orbital 24)	0.1665
15	HOMO -1 for thiophene with COS (eV) (Molecular orbital 36)	-6.917
16	LUMO +1 for thiophene with COS (eV) (Molecular orbital 39)	-1.282
17	$Q_{MULLIKEN}$	$0.0149e^-$
18	Q_{NBO}	$0.00023e^-$

 https://doi.org/10.37896/pd91.5/91565

ISSN: 0369-8963

Frontier molecular orbitals and band gap

The energy of the highest occupied molecular orbital (HOMO) and the lowest unoccupied molecular orbital (LUMO) and band gap (E_g) are calculated at the B3LYP/6-31+G (d) level of theory. The values of HOMO, LUMO, Band gap E_g for thiophene and thiophene with COS are given in Table 1. Figures of molecular orbital of HOMO, LUMO, HOMO-1, and LUMO+1 for isolated thiophene and thiophene with COS at B3LYP/6-31+G(d) are given in Figures 2(a) and 2(b) respectively. The energy difference between HOMO and LUMO is defined as the band gap E_g which indicates the stability and reactivity of the system. The band gap E_g value decreases from 5.97 eV to 5.21eV after COS is physisorbed on thiophene. The decrease of band gap value will increase the electrical conductivity of thiophene. When the band gap value of the complex is decreased after interaction means, it is less chemically stable and more reactive. The molecular orbitals of the first 3 excited states HOMO-LUMO, HOMO-1 to LUMO, and HOMO to LUMO+1 are compared by their energy difference values. Thus the energy required to excite the electron from HOMO (MO 22) to LUMO (MO 23) is 5.97eV for thiophene and, 5.21 eV (MO 37 to MO 38) for thiophene with COS, HOMO-1 (MO 21) to LUMO (MO 23) is 6.37 eV for thiophene and 5.62 eV (MO 36 to MO 38) for the complex. Similarly, the energy required for excitation from HOMO (MO 22) to LUMO +1 (MO 24) is 6.77 eV for the monomer and 5.23 eV (MO 37 to MO 39) for COS physisorbed on thiophene. The general trend for the energy difference for thiophene is HOMO to LUMO < HOMO-1 to LUMO < HOMO to LUMO+1. A different trend is observed for COS adsorbed on thiophene which is given as HOMO to LUMO < HOMO to LUMO+1 < HOMO-1 to LUMO which corresponds to a significant difference in the values of their excitation energies.

 https://doi.org/10.37896/pd91.5/91565

ISSN: 0369-8963

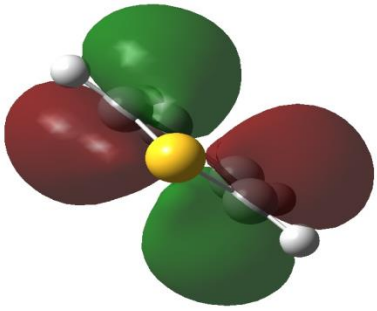

HOMO of thiophene

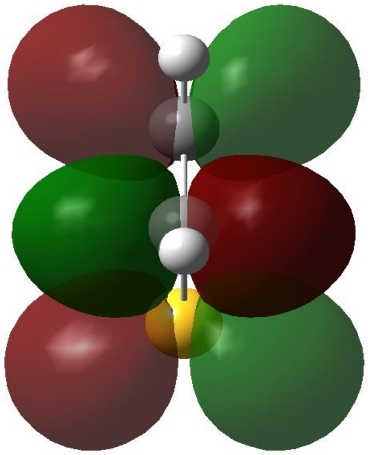

LUMO of thiophene

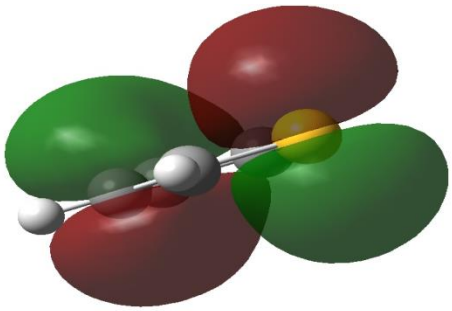

HOMO-1 of thiophene

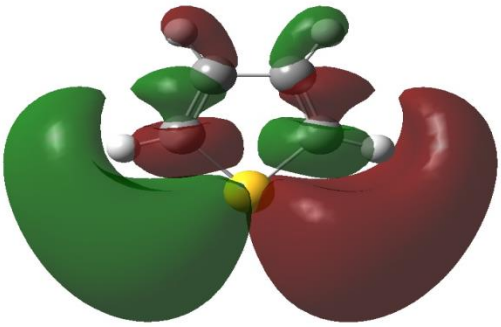

LUMO +1 of thiophene

Figure 2(a). The molecular orbitals of HOMO, LUMO, HOMO-1, and LUMO+1 for isolated thiophene at B3LYP/6-31+G (d) level of theory

https://doi.org/10.37896/pd91.5/91565

ISSN: 0369-8963

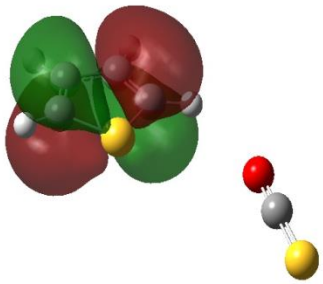

HOMO of thiophene with COS

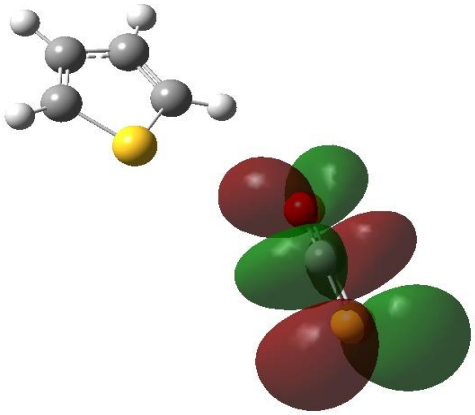

LUMO of thiophene with COS

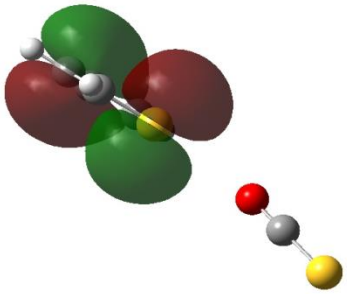

HOMO -1 of thiophene with COS

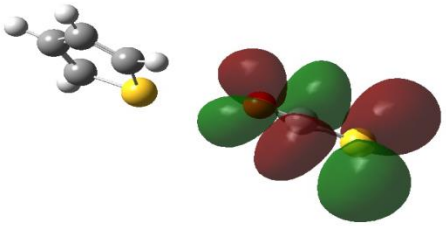

LUMO +1 of thiophene with COS

Figure 2(b). The molecular orbitals of HOMO, LUMO, HOMO-1, and LUMO+1 for thiophene with COS at B3LYP/6-31+G(d) level of theory

 https://doi.org/10.37896/pd91.5/91565

ISSN: 0369-8963

Charge analysis

The population analysis for Mulliken charge transfer showed that COS loses about 0.0149e$^-$ charge to thiophene. According to NBO analysis, COS transfers 0.00023e$^-$ charge to thiophene. The total electron charge distribution for the complex for Mulliken and NBO are shown in Figure 3(a) and 3(b) respectively. The low charge value is related to Van der Waals interaction which is totally in accordance with the value of low interaction energy. The partial charges on the various atoms of the optimized thiophene with physisorbed COS for the Mulliken charges are depicted in Mulliken's plot which can be visualised in Figure 4.

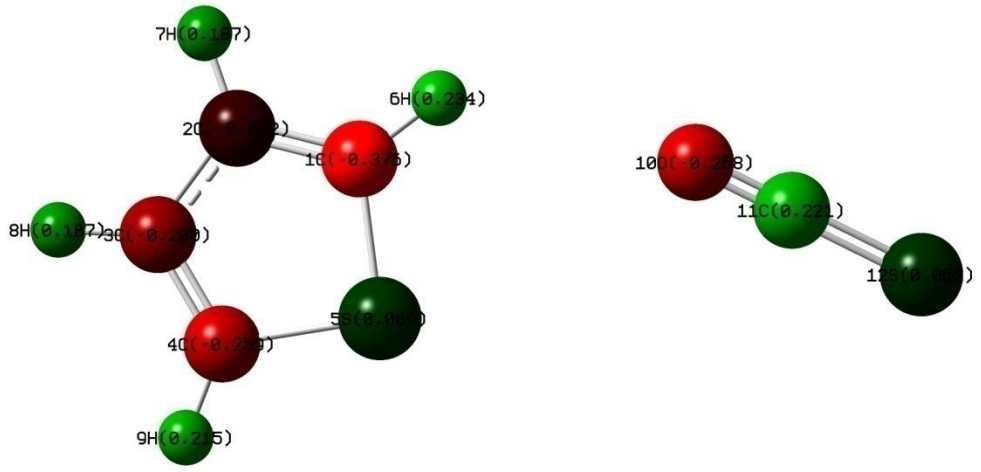

Figure 3(a). The electron charge distribution for thiophene with COS at B3LYP/6-31+G (d) for Mulliken charges

 https://doi.org/10.37896/pd91.5/91565

ISSN: 0369-8963

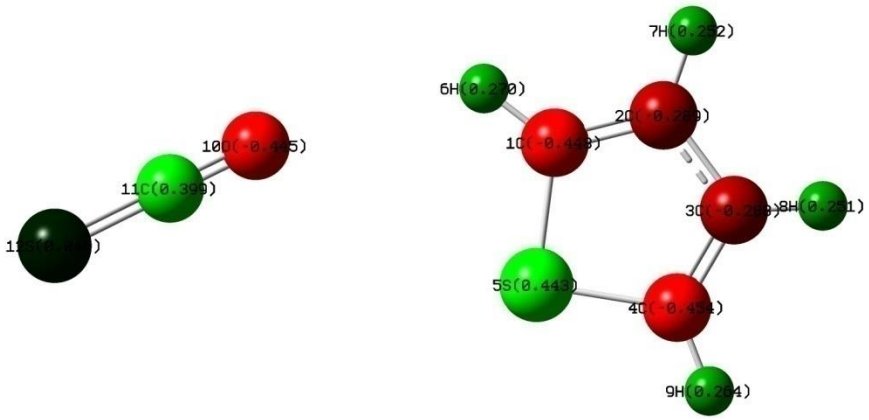

Figure 3(b). NBO total charge distribution (in units of the electron) of thiophene with COS at B3LYP/6-31+G (d) level of theory

 https://doi.org/10.37896/pd91.5/91565

ISSN: 0369-8963

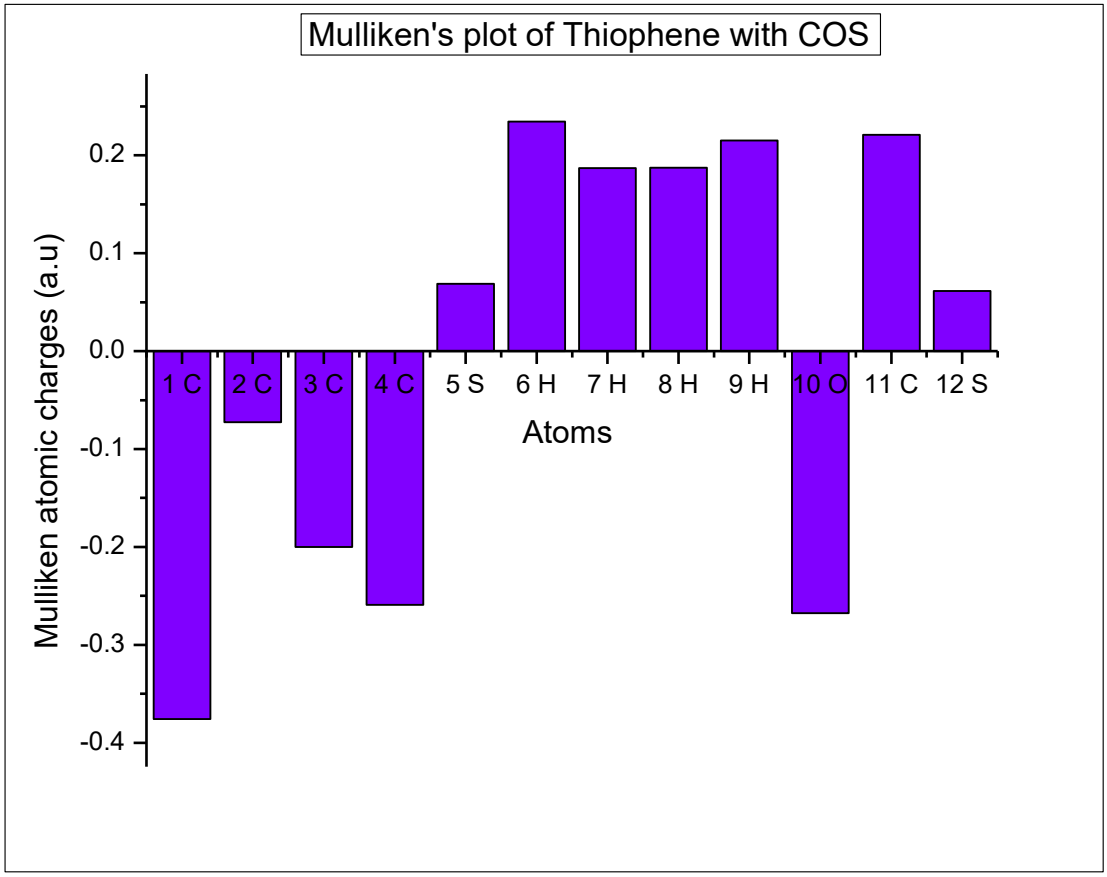

Figure 4. The net atomic charges on various atoms from Mulliken analysis

From the graph, it is seen that C_1 of thiophene has a very more negative charge of -0.37571e, and H_6 of thiophene has more value of the positive charge of 0.234396e, which provides evidence for the charge delocalization in the thiophene. Carbon atoms C_2, C_3, and C_4 show negative charges which indicate that charge gets transferred from COS to thiophene. The maximum value of the negative atomic charge is obtained for C_2 of value -0.07241e. All the hydrogen atoms show positive charges.H_7 (0.187171e) and H_8 (0.187304e) and have only a slight difference in their positive charge values. C_{11} of COS has got a greater positive charge of 0.220882e. Positive charges of 0.061596e and 0.0687e are localized on the S_{12} of COS and S_5 of thiophene respectively. From Fig 4, it is clear that the distribution of partial charges on both COS and thiophene indicates that intermolecular interaction exists between them.

Molecular electrostatic potential analysis

The molecular electrostatic potential (MEP) is a powerful tool for predicting sites and reactivities towards both electrophilic attack and nucleophilic attack properties. The adsorption

 https://doi.org/10.37896/pd91.5/91565

ISSN: 0369-8963

performance of the complex is analysed by the mapping of the total electron density with the molecular electrostatic potential of isolated thiophene and thiophene with COS respectively and are shown in Figures 5(a) and 5(b) respectively. It is evident from Figure 5(b) that there exists a strong surface interaction between COS and thiophene and the monomer has an excellent adsorption effect on COS. Different colors of MEP will represent the various values of the electrostatic surface. The color code of the range is between $-2.311e^{-2}$ (red) and $2.311e^{-2}$ (blue) for thiophene, $-2.319e^{-2}$ (red) and $2.319e^{-2}$ (blue) for COS adsorbed on thiophene. The region of intermediary potential is shown in yellow and green color and the regions of extreme potentials are shown in red and blue colors and are the key indicators of electronegativity. [42]. We can see that the red color of isolated thiophene is dimmed before adsorption. After interaction with COS, the deepest red color because of rich electron density appears in thiophene which results from the reliable transfer of charges from analyte to monomer. The electrostatic potential at different points on the electron density isosurface is shown by coloring the isosurface with contours. Figure 5(c) shows the contour display of the COS adsorbed on thiophene.

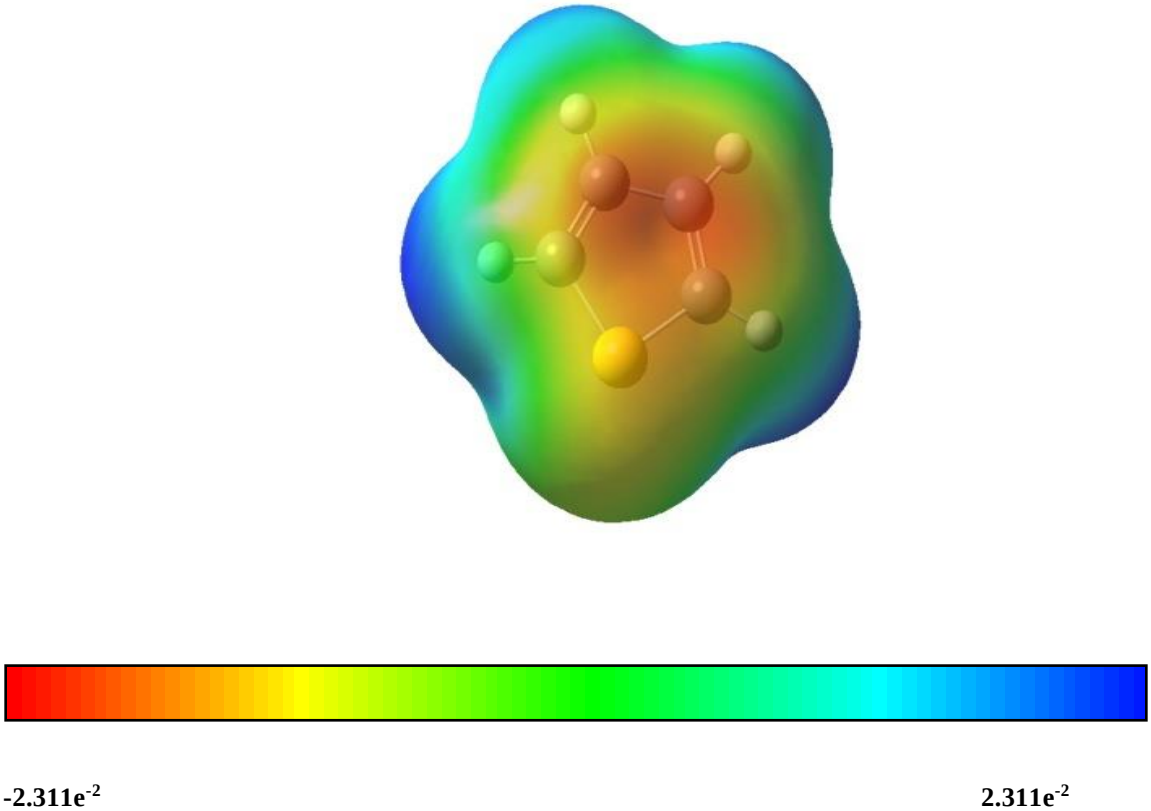

Figure 5(a). The total electron density isosurface mapped with the molecular electrostatic potential of thiophene

 https://doi.org/10.37896/pd91.5/91565

ISSN: 0369-8963

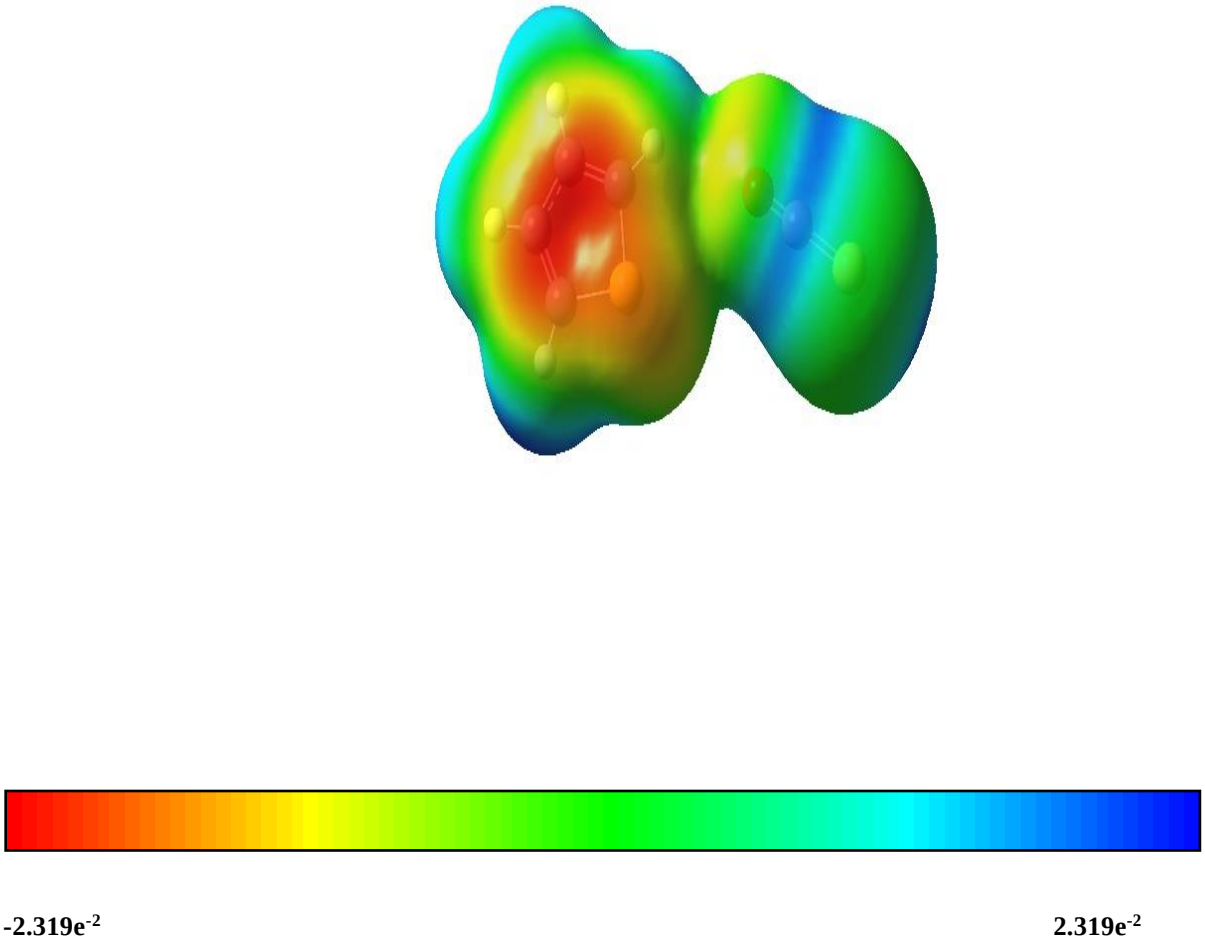

Figure 5(b). The total electron density isosurface mapped with the molecular electrostatic potential of thiophene with adsorbed COS

 https://doi.org/10.37896/pd91.5/91565

ISSN: 0369-8963

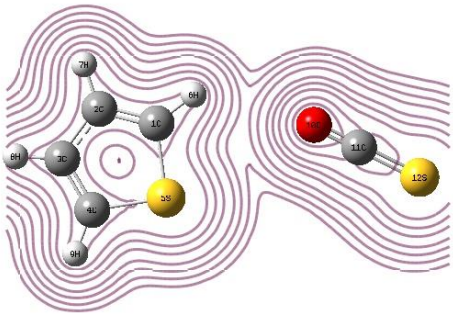

Figure 5(c). Contour display of COS adsorbed on thiophene

Natural atomic orbital and natural bond orbital analysis from

Gaussian NBO version 3.1

Natural atomic orbital analysis

Natural bond orbital (NBO) analysis provides information regarding intramolecular and intermolecular charge transfer. The stability of the molecule which arises from conjugation and hyperconjugation interactions and charges delocalization of the molecular system is analysed using NBO analysis.

The natural atomic orbital (NAO) occupancies, for example, for the C1 carbon atom are given in Table 2. In the table 2 for each of the 19 NAO functions with the corresponding atom attached to it, the angular momentum type (s, px, py, pz, etc), the orbital type (whether core, valence, or Rydberg orbital), the orbital occupancy which is equivalent to the number of electrons or the natural population of the orbital and the orbital energy in Hartrees are given in Table 2. From the table, we can see that for the C1 atom, NAO 6 describes the highest energy Carbon atomic orbital of the "natural minimal basis" (NMB) which is the valence shell having the character of 2px atomic orbital occupied by 1.17929 electrons. The "natural minimal basis" (NMB) always includes the core and valence natural atomic orbitals. From the Table, we infer that the occupancies of the Rydberg NAOs are much lower than core and valence NAOs of the natural minimal basis set. Therefore in explaining the molecular properties, the core and the valence NAO orbitals play a dominant role in the natural minimal basis set than the Rydberg NAOs, which is also evident from Table 2. So Rydberg orbitals are not given much importance. For the C1 carbon atom, NAO 6 is followed by NAO 9 of energy -0.14142

 https://doi.org/10.37896/pd91.5/91565

ISSN: 0369-8963

Hartrees. The natural atomic orbital occupancies with the higher energy of the NMB set for C2, C3, C4, S5, H6, H7, H8, H9 of thiophene and O10, C11, S12 of COS are given in Table 3.

TABLE 2. NATURAL POPULATIONS: Natural atomic orbital occupancies for C1 atom of thiophene

NAO	Atom	No	lang	Type(AO)	Occupancy	Energy
1	C	1	S	Cor(1S)	1.99911	-10.0902
2	C	1	S	Val(2S)	1.05841	-0.27697
3	C	1	S	Ryd(4S)	0.00135	0.91249
4	C	1	S	Ryd(3S)	0.00044	0.48866
5	C	1	S	Ryd(5S)	0.00004	4.19418
6	C	1	px	Val(2p)	1.17929	-0.08497
7	C	1	px	Ryd(4p)	0.00427	0.68553
8	C	1	px	Ryd(3p)	0.00046	0.51239
9	C	1	py	Val(2p)	1.0637	-0.14142
10	C	1	py	Ryd(4p)	0.00485	0.84254
11	C	1	py	Ryd(3p)	0.00058	0.39033
12	C	1	pz	Val(2p)	1.12771	-0.14195
13	C	1	pz	Ryd(4p)	0.00295	0.4772
14	C	1	pz	Ryd(3p)	0.00086	0.38303
15	C	1	dxy	Ryd(3d)	0.00092	2.20417
16	C	1	dxz	Ryd(3d)	0.0006	1.88297
17	C	1	dyz	Ryd(3d)	0.00071	1.73778
18	C	1	dx2y2	Ryd(3d)	0.00128	2.2787
19	C	1	dz2	Ryd(3d)	0.00083	2.11748

 https://doi.org/10.37896/pd91.5/91565

ISSN: 0369-8963

TABLE 3. Natural populations: Natural atomic orbital occupancies with the higher energy of the "Natural Minimal Basis" (NMB) for thiophene and COS

NAO	Atom	No	lang	Type(AO)	Occupancy	Energy
6	C	1	px	Val(2p)	1.17929	-0.08497
28	C	2	py	Val(2p)	1.18589	-0.06165
47	C	3	py	Val(2p)	1.0491	-0.05732
66	C	4	py	Val(2p)	1.21453	-0.0868
88	S	5	py	Val(3p)	1.06698	-0.17818
100	H	6	S	Val(1S)	0.72969	0.09984
102	H	7	S	Val(1S)	0.7478	0.09079
104	H	8	S	Val(1S)	0.74807	0.09004
106	H	9	S	Val(1S)	0.73579	0.08875
119	O	10	pz	Val(2p)	1.56038	-0.3425
132	C	11	px	Val(2p)	0.89449	-0.1177
153	S	12	px	Val(3p)	1.13874	-0.21537

 https://doi.org/10.37896/pd91.5/91565

ISSN: 0369-8963

TABLE 4. Natural population analysis for different orbitals of thiophene with COS

Atom	No	Charge	Core	Valence	Rydberg	Total
C	1	-0.44833	1.99911	4.42911	0.02011	6.44833
C	2	-0.28921	1.99902	4.27325	0.01694	6.28921
C	3	-0.28774	1.99902	4.27167	0.01705	6.28774
C	4	-0.45438	1.9991	4.43513	0.02015	6.45438
S	5	0.44325	9.99899	5.51263	0.04513	15.55675
H	6	0.26966	0	0.72969	0.00065	0.73034
H	7	0.25154	0	0.7478	0.00066	0.74846
H	8	0.25126	0	0.74807	0.00066	0.74874
H	9	0.26371	0	0.73579	0.0005	0.73629
O	10	-0.44494	1.99977	6.4097	0.03547	8.44494
C	11	0.399	1.99965	3.55845	0.0429	5.601
S	12	0.04617	9.99864	5.92715	0.02803	15.95383
TOTAL		0.00000	31.99332	41.77843	0.22825	74.00000

TABLE 5. Percentage of Natural Minimal Basis (NMB) and Natural Rydberg Basis (NRB) Orbitals

Core	31.99332 (99.9791% of 32)
Valence	41.77843 (99.4724% of 42)
Natural Minimal Basis	73.77175 (99.6915% of 74)
Natural Rydberg Basis	0.22825 (0.3085% of 74)

 https://doi.org/10.37896/pd91.5/91565

ISSN: 0369-8963

Table 4 shows the natural atomic charges and total core, valence, and Rydberg populations on each atom and Table 5 shows the percentage of natural minimal basis (NMB) and natural Rydberg basis (NRB) orbitals. From Table 5, it is seen that the high percentage contribution which is greater than 99% is from the natural minimal basis (NMB) set. It is clear that 74 NMB functions from core and valence orbitals contribute 99.6915% whereas 74 Rydberg orbitals of the NRB set to account for only 0.3085% of the total basis set.

Natural bond orbital analysis

Table 6 shows the detailed allocation of Lewis and non-Lewis occupancies into core, valence, and Rydberg orbitals and the percentage of total electron density. The highly occupied NBOs of the natural Lewis structure can be distinguished from the non-Lewis antibonding and Rydberg orbitals in the NBO space by σ_{AB} Lewis (L) and σ^*_{ab} non-Lewis (NL) in the NBO basis. The antibonds (valence shell non-Lewis orbitals) play a vital role in delocalization or the departure from the Lewis orbitals.

TABLE 6. Lewis and non-lewis occupancies into core, valence, and Rydberg shell contributions

Core	31.99332(99.979% of 32)
Valence Lewis	40.30252(95.958% of 42)
Total Lewis	72.29584(97.697% of 74)
Valence non-Lewis	1.58914 (2.147% of 74)
Rydberg non-Lewis	0.11501 (0.155% of 74)
Total non-Lewis	1.70416 (2.303% of 74)

 https://doi.org/10.37896/pd91.5/91565

ISSN: 0369-8963

TABLE 7. Natural atomic orbital occupancies with the percentage of hybrid atomic orbitals of most interacting NBOs.

Parameter	Occupancies	Percentage of NBO on each hybrid		Atomic orbital %
		Hybrid h_A	Hybrid h_B	Hybrid h_A Hybrid h_B
BD (1) C1 - C2	1.98661	50.22%	49.78%	*s(39.29)p(60.67)d(0.04)* *s(34.62)p(65.34)d(0.04)*
BD (2) C1 - C2	1.87931	52.78%	47.22%	*s(0)p(99.95)d(0.05)* *s(0)p (99.95)d (0.05)*
BD (1) C1 - S5	1.98199	51.79%	48.21%	*s(25.40)p(74.47)d(0.14)* *s(18.38)p(80.99)d(0.63)*
BD (1) C1 - H6	1.98632	63.65%	36.35%	*s(35.20)p(64.75)d(0.05)* *s(100)*
BD (1) C2 - C3	1.97904	49.98%	50.02%	*s(33.19)p(66.76)d(0.04)* *s(33.21)p(66.74)d(0.04)*
BD (1) C2 - H7	1.97862	62.67%	37.33%	*s(32.15)p(67.80)d(0.05)* *s(100)*
BD (1) C3 - C4	1.98675	49.76%	50.24%	*s(34.60)p(65.35)d(0.04)* *s(39.33)p(60.63)d(0.04)*
BD (2) C3 - C4	1.88172	46.91%	53.09%	*s(0)p(99.95)d(0.05)* *s(0)p(99.95)d(0.05)*
BD (1) C3 - H8	1.97881	62.66%	37.34%	*s(32.14)p(67.81)d(0.05)* *s(100)*
BD (1) C4 - S5	1.98222	51.99%	48.01%	*s(25.61)p(74.26)d(0.13)* *s(18.23)p(81.14)d(0.64)*
BD (1) C4 - H9	1.98663	63.33%	36.67%	*s(34.94)p(65.01)d(0.05)* *s(100)*
BD (1) O10 - C11	1.99963	66.13%	33.87%	*s(42.91)p(56.51)d(0.58)* *s(40.97)p (58.95)d (0.08)*
BD (2) O10 - C11	1.99831	72.63%	27.37%	*s(0)p(99.64)d(0.36)* *s(0)p(99.86)d(0.14)*
BD (1) C11 - S12	1.99794	58.39%	41.61%	*s(58.97)p(40.95)d(0.09)* *s(18.30)p(80.94)d(0.76)*
LP (1) S5	1.98486	-	-	*s(63.87)p(36.11)d(0.02)*

 https://doi.org/10.37896/pd91.5/91565

ISSN: 0369-8963

LP (2) S5	1.63172	-	-	*s(0)p(99.91)d(0.09)*
LP (1) O10	1.97090	-	-	*s(56.90)p(42.99)d(0.10)*
LP (2) S12	1.57060	-	-	*s(0)p(99.75)d(0.25)*
LP (3) S12	1.56968	-	-	*s(0.01)p(99.73)d(0.26)*
RY*(1) H6	0.00065	-	-	*s(100)*
BD*(2) C1 - C2	0.29297	47.22%	52.78%	*s(0)p(99.95)d(0.05)* *s(0)p (99.95)d(0.05)*
BD*(1) C1 - H6	0.01191	36.35%	63.65%	*s(35.20)p(64.75)d(0.05)* *s(100)*
BD*(2) C3 - C4	0.29637	53.09%	46.91%	*s(0)p(99.95)d(0.05)* *s(0)p (99.95)d (0.05)*
BD*(2) O10 - C11	0.41666	27.37%	72.63%	*s(0)p(99.64)d(0.36)* *s(0)p (99.86)d(0.14)*

Table 7 shows the NBO parameter with its unique label ("BD" for the 2-center bond, "LP" for 1-center valence lone pair, "RY" for 1-center Rydberg, and "BD*" for 2-center antibond, the starred and unstarred label corresponds to Lewis and non-Lewis NBOs respectively). The electron occupancies, the percentage of the NBO on each hybrid for the atoms to which NBO is affixed, and atomic orbital percentage showing the spd composition are given in Table 7. It is evident that each pair of valence hybrids h_A, h_B give rise to a bond σ_{AB} Lewis (L) and antibond σ^*_{ab} non-Lewis (NL) in the NBO basis set. The percentage of hybrid atomic orbitals of bonding orbital O10-C11, C11-S12, lone pair orbitals S5 and O10 shows both s-character and p-character respectively. The remaining bonding orbitals and most of the anti-bonding orbitals are mainly contributed to p-type subshells except the antibonding orbital C1-H6 having the partial contribution of s-type and p-type subshells. It is seen that the Rydberg orbital of the H6 atom is predominantly contributed to the s-type character only.

 https://doi.org/10.37896/pd91.5/91565

ISSN: 0369-8963

TABLE 8. Representation of the NBOs with their coefficients for the hybrids

Parameter	Polarization coefficient C_A		Hybrid label		Representation of the NBO "σ_{cc}"
	Hybrid h_A	Hybrid h_B	Hybrid h_A	Hybrid h_B	
BD (1) C1 - C2	0.7086	0.7056	$sp^{1.54}d^0$	$sp^{1.89}d^0$	σ_{CC}=0.7086($sp^{1.54}d^0$)C1+ 0.7056 ($sp^{1.89}d^0$)C2
BD (1) C1 - S5	0.7197	0.6943	$sp^{2.93}d^{0.01}$	$sp^{4.41}d^{0.03}$	σ_{CC}=0.7197($sp^{2.93}d^{0.01}$)C1+ 0.6943 ($sp^{4.41}d^{0.03}$)S5
BD (1) C2 - C3	0.7069	0.7073	$sp^{2.01}d^0$	$sp^{2.01}d^0$	σ_{CC}=0.7069($sp^{2.01}d^0$)C2+ 0.7073 ($sp^{2.01}d^0$)C3
BD (1) C3 - C4	0.7054	0.7088	$sp^{1.89}d^0$	$sp^{1.54}d^0$	σ_{CC}=0.7054($s^{1.89}d^0$)C3+ 0.7088 ($sp^{1.54}d^0$)C4
BD (1) C4 - S5	0.7210	0.6929	$sp^{2.90}d^{0.01}$	$sp^{4.45}d^{0.04}$	σ_{CC}=0.7210($sp^{2.90}d^{0.01}$)C4+ 0.6929 ($sp^{4.45}d^{0.04}$)S5
BD (1) O10 - C11	0.8132	0.5820	$sp^{1.32}d^{0.01}$	$sp^{1.44}d^0$	σ_{OC}=0.8132($sp^{1.32}d^{0.01}$)O10 +0.5820($sp^{1.44}d^0$)C11
BD (1) C11-S12	0.7461	0.6450	$sp^{0.69}d^0$	$sp^{4.42}d^{0.04}$	σ_{CC}=0.7461($sp^{0.69}d^0$)C11+ 0.6450 ($sp^{4.42}d^{0.04}$)S12

Table 8 denotes the NBOs and the atoms to which NBO is affixed, the polarization coefficients of the hybrids denoted by C_A, the hybrid labels showing the spd composition of each hybrid, and the representation of the NBO with their hybrids which is given by σ. For example bonding natural orbital of sigma type C1-C2 NBO is formed from an $sp^{1.54}d^0$ hybrid (39.29 % s-character, 60.67% p-character and 0.04% d-character) on carbon 1 interacting with an $sp^{1.89}d^0$hybrid (34.62 % s-character, 65.34% p-character and 0.04% d-character on carbon 2 is given by equation (3.1)

σ_{CC}=0.7086($sp^{1.54}d^0$)C1+ 0.7056 ($sp^{1.89}d^0$)C2……..(3.1)

Second-order perturbation theory analysis of Fock matrix in NBO basis

Energetic analysis of NBO interactions is based on the availability of a 1-electron effective energy operator called the Fock matrix and the estimates of energetic importance based on II order perturbation theory are calculated. It is a well-known fact that some orbitals are electron

 https://doi.org/10.37896/pd91.5/91565

ISSN: 0369-8963

donors and some orbitals are electron acceptors. The hyperconjugative interaction energy and the electron density transfer from the filled orbitals to vacant orbitals are analysed using the second-order perturbation theory using the Fock matrix.

From the second-order perturbation theory, for each donor, NBO (i) and acceptor NBO (j), the hyperconjugative interaction energy $E^{(2)}$ associated with delocalization can be deducted using the formula given by equation (3.2)

$$E^{(2)} = \Delta E_{ij} = \frac{q_i F(i,j)^2}{\varepsilon_j - \varepsilon_i} \qquad \ldots\ldots\ldots\ldots\ldots\ldots\ldots\ldots\ldots\ldots (3.2)$$

where q_i is the donor orbital occupancy, ε_j, ε_i are diagonal elements (orbital energies), and F(i,j) is the off-diagonal NBO Fock matrix element. Table 9 explains the 'donor-acceptor' which is also called 'bond-antibond interactions' on the NBO basis by using the Fock matrix. Our findings investigate the interaction between filled donor Lewis type NBOs and empty acceptor non-Lewis type NBOs. The interactions lead to loss of occupancy from the localized NBOs of the idealized Lewis structure into the empty non-Lewis orbitals by delocalizations or departure from the idealized Lewis structure.

Table 9 presents the second-order perturbation energies of the Fock matrix of NBOs of thiophene. For intramolecular interaction, the entries are included in the table only when the interaction energy exceeds a default threshold of 0.50 kcal/mol. Out of all the interacting NBOs, the interaction between the sulfur lone pair and the π* (C3-C4) is seen to give the strongest stabilization energy of 21.28 kcal/mol. The next strongest stabilization energy of 21.18 kcal/mol is identified for the interaction of lone pair orbital localized on S5 with the π*(C1-C2). Thus the interaction energy that leads to stabilization which arises from the nonbonding interactions increases the stability of the monomer. [43]. The delocalization of electrons from π (C1-C2) to π* (C3-C4) resulted in the strongest stabilization energy of 15.63kcal/mol. The other interaction due to the delocalization of electrons of π(C3-C4)to π*(C1-C2) gave stronger stabilization energy of 15.32 kcal/mol. Thus higher $E^{(2)}$ of thiophene originates from the atomic overlap between LP(S) to π*(C-C) orbitals and between Π (C-C) to π* (C-C) confirming higher intramolecular charge transfer within the molecule. When the stabilization energy is large, the interaction between the electron donors and acceptors will be more which means there is a tendency for the electron donors to donate more electrons to acceptors which will increase the extent of conjugation of the system. [44]. This can be identified with increased electron density stabilizing the donor-acceptor interaction.

The second-order perturbation theory analysis of the Fock matrix of interacting NBOs of monomer with the analyte is presented in Table 10. It is mentioned in the output result of NBO that the entries are included in the Table 10 which corresponds to the intermolecular threshold of 0.05kcal/mol. The NBO analysis of the interaction of thiophene with COS showed that there were only two interactions that correspond to intermolecular interactions (unit-2 to unit-1) and are mentioned in table 10. The strongest interaction of the lone pair of O10 with antibonding C1-H6 has stabilized the complex thiophene with COS by 0.23kcal/mol. Another intermolecular interaction between bonding orbital O10-C11 and Rydberg non –Lewis NBO of H6 caused stabilization of 0.05kcal/mol. It is very clear that the transfer of electrons from LP O10 of COS (donor NBO) to σ*(C1-H6) of thiophene (acceptor NBO) has greatly stabilized

 https://doi.org/10.37896/pd91.5/91565

ISSN: 0369-8963

the complex monomer with the analyte. It is found that the charge transfer between analyte and monomer is due to overlapping of out of phase interaction that forms the antibonding of σ* type of C_1-H6 of thiophene with lone electron pair of oxygen of COS. Thus in the case of thiophene with COS, on adsorption, the molecular interactions are identified from the atomic overlap between LP(O) to σ*(C1-H6). From the output result of NBO analysis it is stated that from unit-1 (thiophene) to unit-2 (COS), no entries are included in the table because there is no such transfer of electrons above the threshold value. We already stated that COS loses electrons to thiophene from Mulliken's analysis. Thus the NBO analysis also substantiates our result that COS is a donor NBO and thiophene is an acceptor NBO. Thus, it is seen from Tables 9 and 10, the interaction of the orbitals leads to hyperconjugation of the system which results in the intramolecular and intermolecular charge transfer (ICT) causing the stabilization of the system.

 https://doi.org/10.37896/pd91.5/91565

ISSN: 0369-8963

TABLE 9. Second-order perturbation theory analysis of Fock matrix of thiophene by NBO analysis

Within unit 1 (for thiophene)

The threshold for printing: 0.50 kcal/mol

Donor NBO (i)	Acceptor NBO (j)	$E^{(2)}$ kcal/mol	E(j)-E(i) a.u.	F(i,j) a.u.
σ(C1-C2)	σ* (C1-H6)	1.73	1.2	0.041
σ(C1-C2)	σ* (C2-C3)	2	1.25	0.045
σ(C1-C2)	σ* (C2-H7)	1.46	1.19	0.037
σ(C1-C2)	σ* (C3-H8)	2.67	1.19	0.05
σ(C1-C2)	σ* (C4-S5)	0.5	0.95	0.02
Π (C1-C2)	π* (C3-C4)	15.63	0.29	0.063
σ (C1-S5)	σ*(C2-H7)	4.02	1.12	0.06
σ (C1-S5)	σ*(C3-C4)	0.66	1.24	0.026
σ (C1-S5)	σ*(C4-H9)	2.73	1.12	0.049
σ (C1-H6)	σ*(C1-C2)	2	1.14	0.043
σ (C1-H6)	σ*(C2-C3)	2.67	1.08	0.048
σ(C1-H6)	σ*(C4-S5)	0.53	0.78	0.018
σ(C2-C3)	σ*(C1-C2)	1.93	1.26	0.044
σ(C2-C3)	σ*(C1-H6)	3.57	1.14	0.057
σ(C2-C3)	σ*(C2-H7)	0.86	1.13	0.028
σ(C2-C3)	σ*(C3-C4)	1.95	1.25	0.044
σ(C2-C3)	σ*(C3-H8)	0.86	1.13	0.028
σ (C2-C3)	σ*(C4-H9)	3.59	1.13	0.057
σ (C2-H7)	σ*(C1-C2)	1.61	1.12	0.038

 https://doi.org/10.37896/pd91.5/91565

ISSN: 0369-8963

σ (C2-H7)	σ*(C1-S5)	3.8	0.76	0.048
σ (C2-H7)	σ*(C2-C3)	0.55	1.06	0.021
σ (C2-H7)	σ*(C3-C4)	1.87	1.12	0.041
σ (C3-C4)	σ*(C1-S5)	0.51	0.95	0.02
σ (C3-C4)	σ*(C2-C3)	2	1.25	0.045
σ (C3-C4)	σ*(C2-H7)	2.67	1.19	0.05
σ (C3-C4)	σ*(C3-H8)	1.46	1.19	0.037
σ (C3-C4)	σ*(C4-H9)	1.74	1.19	0.041
π (C3-C4)	π*(C1-C2)	15.32	0.29	0.062
σ (C3-H8)	σ*(C1-C2)	1.85	1.12	0.041
σ (C3-H8)	σ*(C2-C3)	0.55	1.06	0.022
σ (C3-H8)	σ*(C3-C4)	1.61	1.12	0.038
σ (C3-H8)	σ*(C4-S5)	3.77	0.76	0.048
σ (C4-S5)	σ*(C1-C2)	0.64	1.25	0.025
σ (C4-S5)	σ*(C1-H6)	2.7	1.13	0.049
σ (C4-S5)	σ*(C3-H8)	4.02	1.12	0.06
σ (C4-H9)	σ*(C1-S5)	0.52	0.78	0.018
σ (C4-H9)	σ*(C2-C3)	2.64	1.08	0.048
σ (C4-H9)	σ*(C3-C4)	1.97	1.15	0.042
LP(1)S5	σ*(C1-C2)	1.95	1.24	0.044
LP(1)S5	σ*(C3-C4)	1.97	1.23	0.044
LP(2)S5	π*(C1-C2)	21.18	0.26	0.068
LP(2)S5	π*(C3-C4)	21.28	0.26	0.068

 https://doi.org/10.37896/pd91.5/91565

ISSN: 0369-8963

TABLE 10. Second-order perturbation theory analysis of Fock matrix of thiophene with COS by NBO analysis

From unit2 to unit1 (from COS to thiophene)

(Intermolecular threshold: 0.05 kcal/mol)

Donor NBO (i)	Acceptor NBO (j)	$E^{(2)}$ kcal/mol	E(j)-E(i) a.u.	F(i,j) a.u.
σ(O10- C11)	RY*(1) H6	0.05	1.86	0.009
LP (1) O10	σ*(C1-H6)	0.23	1.25	0.015

From unit 1 to unit 2 (from thiophene to COS)
None above threshold

Conclusion

DFT calculations at B3LYP/6-31+G(d) and ωB97XD/6-31+G(d) level of theory of thiophene with COS are carried out to investigate the thiophene as a good toxic gas sensing material. The intermolecular interaction energies are determined and are counterpoise corrected. Our findings elucidate that the intermolecular interaction is found to be of weak Van der Waals interaction. Thus our calculation revealed a physisorption process between COS and thiophene due to its low adsorption energy. The Mulliken and NBO charge transfer are interpreted and the results demonstrate that the charge gets transferred from COS to thiophene. Frontier molecular orbital studies are visualised and it provides evidence of overlapping of atomic orbitals. The bandgap value of thiophene decreases upon interaction with thiophene increasing its conductivity. Molecular Electrostatic Potential energy (MEP) analysis is carried out to know about the nature of the interaction between the analyte and the monomer. MEP surface studies provide information regarding the charge density distribution before and after the interaction of COS with the analyte. The intramolecular and intermolecular charge transfer that occurs between the bonding and the antibonding orbital is determined by NBO calculation. The natural population analysis is performed to know about the accumulation of electrons in the core, valence, and Rydberg subshell of their atomic orbitals. The hybridization details and the contribution of electrons to s-type and p-type subshells are reported by NBO analysis. The second-order perturbation analysis is consistent with our result of COS as a donor and

 https://doi.org/10.37896/pd91.5/91565

ISSN: 0369-8963

thiophene as an acceptor. NBO analysis reflects the intramolecular and intermolecular charge transfer (ICT) that arise from hyperconjugative interactions leading to the strongest stabilization energy. Thus, in the future, the gas sensing properties of thiophene with COS are used in analyzing the applications of thiophene in various fields of organic electronics and optoelectronics.

Acknowledgments

The authors are very much grateful to KCG College of Technology, Karapakkam and Madras Christian College, Tambaram for providing the computational facilities to carry out this work.

REFERENCES

1. S. Bibi, H. Ullah, S. M. Ahmad, A. U. H. Ali Shah, S. Bilal, A. A. Tahir, K. Ayub, Molecular and electronic structure elucidation of polypyrrole gas sensors. *J. Phys. Chem. C*. 119, 15994–16003 (2015).

2. A. S. Rad, P. Valipour, A. Gholizade, S. E. Mousavinezhad, Interaction of SO2 and SO3 on terthiophene (as a model of polythiophene gas sensor): DFT calculations. *Chem. Phys. Lett*. 639, 29–35 (2015).

3. A. S. Rad, A. S. Rad, Terthiophene as a model sensor for some atmospheric gases : theoretical study Terthiophene as a model sensor for some atmospheric gases : theoretical study. 8976 (2016), doi:10.1080/00268976.2015.1102348.

4. A. Shokuhi Rad, S. Ghasemi Ateni, H. A. Tayebi, P. Valipour, V. Pouralijan Foukolaei, First-principles DFT study of SO2 and SO3 adsorption on 2PANI: a model for polyaniline response. *J. Sulfur Chem.* 37, 622–631 (2016).

5. H. Sajid, T. Mahmood, K. Ayub, An accurate comparative theoretical study of the interaction of furan, pyrrole, and thiophene with various gaseous analytes. *J. Mol. Model.* 23, 1–18 (2017).

6. A. Shokuhi Rad, Application of polythiophene to methanol vapor detection: an ab initio study. *J. Mol. Model.* 21, 2–7 (2015).

7. A. Shokuhi Rad, M. Esfahanian, E. Ganjian, H. allah Tayebi, S. B. Novir, The polythiophene molecular segment as a sensor model for H2O, HCN, NH3, SO3, and H2S: a density functional theory study. *J. Mol. Model.* 22, 1–8 (2016).

8. H. Ullah, A. U. H. A. Shah, S. Bilal, K. Ayub, DFT study of polyaniline NH3, CO2, and CO gas sensors: Comparison with recent experimental data. *J. Phys. Chem. C*. 117, 23701–23711 (2013).

9. A. Shokuhi, N. Nasimi, M. Jafari, D. Sadeghi, Sensors and Actuators B : Chemical Ab-initio study of interaction of some atmospheric gases (SO 2 , NH 3 , H 2 O , CO , CH 4 and CO 2) with polypyrrole (3PPy) gas sensor : DFT calculations. *Sensors Actuators B. Chem.* 220, 641–651 (2015).

 https://doi.org/10.37896/pd91.5/91565

ISSN: 0369-8963

10. T. Patois, J. B. Sanchez, F. Berger, J. Y. Rauch, P. Fievet, B. Lakard, Ammonia gas sensors based on polypyrrole films: Influence of electrodeposition parameters. *Sensors Actuators, B Chem.* 171–172, 431–439 (2012).

11. H. Ullah, K. Ayub, Z. Ullah, M. Hanif, R. Nawaz, A. A. Shah, S. Bilal, Theoretical insight of polypyrrole ammonia gas sensor. 172, 14–20 (2013).

12. A. Shokuhi, S. Sadeghi, S. Mohseni, Journal of Solid State Chemistry Study on the adsorption properties of O 3 , SO 2 , and SO 3 on B-doped graphene using DFT calculations. *J. Solid State Chem.* 237, 204–210 (2016).

13. X. Gao, Q. Zhou, J. Wang, L. Xu, W. Zeng, Performance of Intrinsic and Modified Graphene for the Adsorption of H2S and CH4: A DFT Study. *Nanomater. 2020, Vol. 10, Page 299*. 10, 299 (2020).

14. Z. Zhao, Y. Yong, Q. Zhou, Y. Kuang, X. Li, Gas-Sensing Properties of the SiC Monolayer and Bilayer: A Density Functional Theory Study. *ACS Omega*. 5, 12364–12373 (2020).

15. S. S. Varghese, S. Swaminathan, K. K. Singh, V. Mittal, Ab initio study on gas sensing properties of group III (B, Al and Ga) doped graphene. *Comput. Condens. Matter*. 9, 40–55 (2016).

16. K. Imani, G. Jafari, M. R. Abolhasani, Electronic Structure Calculation of Adsorbate Gas Molecules on an Armchair Graphene Nanoribbon. *ISRN Condens. Matter Phys.* 2012, 1–5 (2012).

17. S. S. Pandule, S. U. Shisodia, R. P. Pawar, V. V Chabukswar, S. S. Pandule, S. U. Shisodia, R. P. Pawar, V. V Chabukswar, Synthesis , Properties , and Ammonia Gas Sensing Applications of Poly- [1- (4-nitronaphthalen-1-. *Polym. Plast. Technol. Eng.* 56, 268–275 (2018).

18. Y. T. Yu, S. M. Majhi, H. G. Song, Synthesis and Gas Sensing Properties of Au@In2O3 Core-shell Nanoparticles. *Procedia Eng.* 168, 227–230 (2016).

19. G. Chimowa, Z. P. Tshabalala, A. A. Akande, G. Bepete, B. Mwakikunga, S. S. Ray, E. M. Benecha, Improving methane gas sensing properties of multi-walled carbon nanotubes by vanadium oxide filling. *Sensors Actuators B Chem.* 247, 11–18 (2017).

20. J. Ren, W. Kong, J. Ni, The Potential Application of BAs for a Gas Sensor for Detecting SO2 Gas Molecule: a DFT Study. *Nanoscale Res. Lett.* 14, 0–6 (2019).

21. M. Li, H. Zhu, G. Wei, A. He, Y. Liu, DFT calculation and analysis of the gas sensing mechanism of methoxy propanol on Ag decorated SnO2 (110) surface. *RSC Adv.* 9, 35862–35871 (2019).

22. S. S. Liu, L. J. Bian, F. Luan, M. T. Sun, X. X. Liu, Theoretical study on polyaniline gas sensors: Examinations of response mechanism for alcohol. *Synth. Met.* 162, 862–867 (2012).

 https://doi.org/10.37896/pd91.5/91565

ISSN: 0369-8963

23. G. A. Hudson, L. Cheng, J. Yu, Y. Yan, D. J. Dyer, M. E. McCarroll, L. Wang, Computational studies on response and binding selectivity of fluorescence sensors. *J. Phys. Chem. B.* 114, 870–876 (2010).

24. A. Ramanavičius, A. Ramanavičiene, A. Malinauskas, Electrochemical sensors based on conducting polymer—polypyrrole. *Electrochim. Acta*. 51, 6025–6037 (2006).

25. S. Yang, P. Olishevski, M. Kertesz, Bandgap calculations for conjugated polymers. *Synth. Met.* 141, 171–177 (2004).

26. S. S. Zade, M. Bendikov, From oligomers to polymer: Convergence in the HOMO-LUMO gaps of conjugated oligomers. *Org. Lett.* 8, 5243–5246 (2006).

27. G. Li, T. Wang, A. Schulz, S. Bhosale, M. Lauer, Porphyrin – acetylene – thiophene polymer wires †. 1, 552–553 (2004).

28. A. El Alamy, A. Amine, S. M. Bouzzine, M. Lachgar, M. Hamidi, A. Elhamzi, M. Bouachrine, DFT study of small compounds based on thiophene and benzo[1,2,5] thiadiazole for solar cells: Correlation-structure / electronic properties. *J. Mater. Environ. Sci.* 8, 3897–3905 (2017).

29. J. H. Wat, G. Griffin, Extrapolating the {Excitation} {Energy} of {Polythiophene} from {Thiophene} {Oligomers}. 8, 9 (2019).

30. A. El Alamy, A. Amine, M. Bouachrine, DFT study of electronic and optical properties of small oligothiophenes based on terthiophene end-capped by several donor groups. *Orbital*. 9, 188–196 (2017).

31. C. P. Chengelis, R. A. Neal, Studies of carbonyl sulfide toxicity: Metabolism by carbonic anhydrase. *Toxicol. Appl. Pharmacol.* 55, 198–202 (1980).

32. E. Health, H. Assessment, Air Toxics Hot Spots Program Carbonyl Sulfide Reference Exposure Levels (2017).

33. A. R. Bartholomaeus, V. S. Haritos, Review of the toxicology of carbonyl sulfide , a new grain fumigant. 43, 1687–1701 (2005).

34. Frisch, M. J. T. G. W.; Schlegel, H. B.; Scuseria, G. E.; Robb, M. A.; Cheeseman, J. R.; Scalmani, G.; Barone, V.; Mennucci, B.; Petersson, G. A.; et al. Gaussian 09, Rev. D. 0.1; Gaussian, Inc.: Wallingford, CT, 2013.

35. Dennington, Roy; Keith, Todd; Millam J (2009) GaussView 5.0. Semichem Inc, Shawnee Mission, KS

36. A. D. Becke, Density-functional thermochemistry. III. The role of exact exchange. *J. Chem. Phys.* 98, 5648–5652 (1993).

37. Becke, A.D. (1998) Density-Functional Exchange-Energy Approximation with Correct Asymptotic Behavior. Physical Review A, 38, 3098-3100.

 https://doi.org/10.37896/pd91.5/91565

ISSN: 0369-8963

38. C. Lee, W. Yang, R. G. Parr, Development of the Colle-Salvetti correlation-energy formula into a functional of the electron density. *Phys. Rev. B.* 37, 785–789 (1988).

39. B. Miehlich, A. Savin, H. Stoll, H. Preuss, Results obtained with the correlation energy density functionals of becke and Lee, Yang and Parr. *Chem. Phys. Lett.* 157, 200–206 (1989).

40. S. Grimme, Density functional theory with London dispersion corrections. *Wiley Interdiscip. Rev. Comput. Mol. Sci.* 1, 211–228 (2011).

41. A. D. Boese, Density Functional Theory and Hydrogen Bonds: Are We There Yet? *ChemPhysChem*. 16, 978–985 (2015).

42. J. I. Panneerdoss, J. S. Jeyakumar, UV and Visible) Investigation, Optical and Physico Chemical Property Analysis on In 2 O 3 Thin Films. *J Theor Comput Sci*. 2, 120 (2015).

43. V. Balachandran, T. Karthick, S. Perumal, A. Nataraj, Comparative theoretical studies on natural atomic orbitals, natural bond orbitals and simulated UV-visible spectra of N-(methyl)phthalimide and N-(2 bromoethyl)phthalimide. *Indian J. Pure Appl. Phys.* 51, 178–184 (2013).

44. N. Prabavathi, S. N. N, V. Krishnakumar, Spectroscopic Investigation (FT-IR, FT-Raman, NMR and UV-Vis),Conformational Stability, NBO and Thermodynamic Analysis of 1-(2-Methoxyphenyl) Piperazine and 1-(2-Chlorophenyl) Piperazine by DFT Approach. *Pharm. Anal. Acta*. 06, 1–20 (2015).

 https://doi.org/10.37896/pd91.5/91565